Global and Planetary Change 168 (2018) 67–77

Contents lists available at ScienceDirect

Global and Planetary Change

journal homepage: www.elsevier.com/locate/gloplacha

Research article

# Statistical reconstruction of global vegetation for the last glacial maximum

Yaping Shao*, Andreas Anhäuser, Patrick Ludwig, Philipp Schlüter, Ehimen Williams

*Institute for Geophysics and Meteorology, University of Cologne, Germany*

ABSTRACT

We provide an estimate of global vegetation density for the Last Glacial Maximum (LGM) using a simple statistic model. For today's climate, vegetation is divided into 11 vegetation types plus bare soil, for each of which an empirical relationship between the probability of its occurrence and climate controls is derived. The relationships are then used to reconstruct the glacial vegetation patterns with and without considering $CO_2$ modifications. For the LGM, the climate drivers are estimated from an ensemble-average of global paleo-climate simulations. The reconstruction suggests that vegetation types existing in today's cooler and drier regimes prevailed during the LGM and today's desert areas had more vegetation then. The vegetation patterns of the Amazon and Sahara are examined in detail. In the Amazon, tropical rainforest cover is reduced from 80% in today's climate to 40% in the LGM climate. The Sahara was partly covered by shrubs and grassland, with bare ground fraction reduced from 80% today to 30% in the LGM. The reconstructed vegetation patterns are compared with available biome data.

## 1. Introduction

Vegetation plays a major role in the global energy, water, carbon and dust cycles and is important to atmosphere and land surface interactions. Over time, due to the different climate and $CO_2$ conditions, vegetation has also been changing. In this study, we present a probabilistic estimate of vegetation cover in the Last Glacial Maximum (LGM) and study how they might have changed from the LGM to today.

The LGM is the time in the last glacial period (110–12 ka BP, thousands of years Before Present) when the global ice cover reached its maximum extent. While Mix et al. (2001) and Harrison et al. (2014) dated the LGM to 23–19 ka BP, Clark et al. (2009) suggested that the maximum ice sheet extent occurred more likely between 33 and 26 ka BP. Given the still limited capacity of the global climate models (GCMs) in paleoclimate simulation, the term LGM in this study simply refers to an equilibrium state of the glacial climate. Since the Younger Dryas (11 ka BP), the Earth's climate entered an interglacial period (the Holocene) marked by warmer temperatures (Taylor et al., 1997). Associated with the climate shift, the vegetation patterns also underwent profound changes.

Existing studies on vegetation in the LGM are mostly based on pollen records (Bigelow et al., 2003; Binney et al., 2016) and models (Woillez et al., 2011). Only a few global vegetation maps for the LGM have been compiled, e.g., in the CLIMAP (Climate: Long range Investigation, Mapping, and Prediction, 1984) project, by Ray and Adams (2001). A more recent synopsis, but not designed to obtain fully global coverage, is available from the Paleo-vegetation Mapping Project (known as BIOME 6000, Prentice and Webb III, 1998; Prentice et al., 2000).

In GCMs and Earth System Models (ESMs), e.g., those participating in the 3rd Phase of the Paleoclimate Modeling Inter-comparison Project (PMIP3, Braconnot et al., 2012), vegetation is either prescribed to the pre-Industrial conditions or simulated using vegetation models. Dynamic and statistic vegetation models of different complexities have been developed (e.g. ORCHIDEE, Krinner et al., 2005; JSBACH, Raddatz et al., 2007). A dynamic model predicts vegetation by integration of a land-surface model with modules for vegetation growth and soil nutrients (Parton et al., 1993; Dickinson et al., 2006). The difficulty of using such models is that a list of input parameters is required, that are not known. Although the vegetation models used for the GCM/ESM simulations are less complex, the need of parameter specification remains formidable. As a consequence, large discrepancies occur among the pre-specified and/or simulated vegetation types and covers (Supplement S1, Fig. S1). Some models predicted higher tree-cover fraction for the LGM than for the preindustrial climate, e.g., across central Europe, in contradiction to the reconstruction of Ray and Adams (2001).

With the recent increase of activities in regional paleo-climate modeling, the need for high-resolution paleo-vegetation data on regional scales has become obvious (Ludwig et al., 2016, 2017), which are not readily available from dynamic vegetation models or proxies. Our first motivation for this study arises thus from the need of better

* Corresponding author.
*E-mail address:* yshao@uni-koeln.de (Y. Shao).

https://doi.org/10.1016/j.gloplacha.2018.06.002
Received 2 December 2017; Received in revised form 5 June 2018; Accepted 7 June 2018
Available online 15 June 2018
0921-8181/ 

vegetation representation for regional paleo-climate modeling to simulate atmosphere and land surface feedbacks (Strandberg et al., 2011; Ludwig et al., 2017).

Our second motivation arises from the need for specifying paleo-vegetation in studying its effects on human existence. The LGM is a milestone in the history of human evolution (Maier et al., 2016). The transition from the LGM to the Holocene saw a rapid development of the hunter-gatherer groups to sedentary agricultural societies, which led to population agglomeration and set the foundation of the modern civilization (Skoglund et al., 2012). The changes of the ecosystems associated with the climate change played a major role in this, because human existence depended on vegetation. Maier et al. (2016) showed that the areas of high population density of hunter-gatherers in Europe during the LGM correspond well with the areas of favorable climate conditions. Thus, the knowledge of the LGM vegetation, is critical for understanding the development of hunter-gatherer societies. For this kind of studies, a simple and robust vegetation model is often sufficient and preferable.

In this study, we reconstruct the global vegetation cover for the LGM using a simple probabilistic approach. Following the *International Geosphere-Biosphere Program* (IGBP), vegetation is classified into 11 types plus bare soil. For each type, a statistical relationship is derived between the probability of its existence and climate controls which influences vegetation. Atmospheric $CO_2$ concentration ($CO_2$ hereafter) also impacts on plant growth, as the levels of $CO_2$ affect the water-, light- and nutrient-use efficiencies and the photosynthetic rate of plants. In particular, the relative photosynthetic responses of the $C_3$ and $C_4$ plants to $CO_2$ changes need to be considered (Bond et al., 2003). $CO_2$ has been on the rise from 160 to 200 ppm in the LGM to ~275 ppm in the Holocene and reached ~407 ppm in 2017 (Tans, 2018). The $CO_2$ increase may have changed the abundances of the $C_3$ plants in Earth's vegetation (Polley et al., 1993; Jolly and Haxeltine, 1997; Collatz et al., 1998; Levis et al., 1999; Cowling et al., 2001). Harrison and Prentice (2003) examined vegetation response to climate and $CO_2$ changes between the LGM and today using model simulations. They reported that the low $CO_2$ during the LGM restricted the extent of forests, especially in the tropics where forests lost ground to grasses, shrubs and savannas. Thus, today's vegetation-climate relationships may require modification before applied to the LGM (Guiot et al., 1999).

While the vegetation responses to climate and $CO_2$ changes are complex, based on the results of Woillez et al. (2011), we found climate change explains about 75% of the variance of the simulated vegetation difference between the modern (with $CO_2$ = 310 ppm) and LGM (with $CO_2$ = 185 ppm) times, while $CO_2$ change explains about 25%. The simulations of Izumi and Lézine (2016) showed that, for a given climate, the dependence of vegetation growth on $CO_2$ appears to be quite linear. Thus, it is justifiable to apply today's vegetation-climate relationships, with relatively simple corrections for $CO_2$, to estimate the vegetation cover for the LGM. To test our model, we first apply it to today's climate and compare the simulated vegetation cover with satellite data. For the LGM, some pollen data exist (Harrison, 2017) from which biomes can be estimated and used for model comparison. Based on the model results, we discuss the differences in vegetation cover between the LGM and today.

## 2. Method and data

### 2.1. Statistic method for vegetation reconstruction

We assume the vegetation-climate-$CO_2$ relationships do not change with time and thus, past vegetation can be reconstructed by transferring today's relations to paleo-climate conditions. We first consider the vegetation-climate relationships and then modify them by accounting for the $CO_2$ differences between today and the LGM. For simplicity, a classification by vegetation types (e.g. needleleaf forest) rather than by plant species (e.g. *Pinus massoniana*) is widely adopted in climate modeling. Following the IGBP classification, vegetation is divided into 12 types, namely: (1) evergreen needleleaf forest; (2) evergreen broadleaf forest; (3) deciduous needleleaf forest; (4) deciduous broadleaf forest; (5) mixed forest; (6) woodland; (7) wooded grassland; (8) closed shrubland; (9) open shrubland; (10) grassland and (11) cultivated and managed land, and (12) bare ground. For analysis of vegetation cover in the LGM, the IGBP classification of today's anthropogenic vegetation (i.e., type (11)) is excluded.

Several vegetation types may occur with different frequencies in the same climate zone. For vegetation type $i$, we denote the probability of its occurrence as $P_i$ (vegetation probability, hereafter) and assume that the vegetation probability density function (PDF) $p_i$ is a function of $J$ climate controls $C_j$ ($j$ = 1, …, $J$), namely, $p_i(C_j)$. We refer to the vegetation PDF, $p_i(C_j)$, as a vegetation-climate model (VC-model). Various combinations of climate controls are possible. If we use precipitation, $R$, and temperature, $T$, as climate controls, then the VC-model can be denoted as $p_i(R, T)$.

Vegetation density, $\sigma_i$, is the fraction of land surface covered by vegetation type $i$. For a location ($x$, $y$), it is identical to vegetation probability, i.e.

$$\sigma_i(x,y) \equiv P_i(x,y) = \int p_i(R(x,y), T(x,y))\mathrm{dRdT} \quad (1)$$

and satisfies the constraint

$$\sum_{i=1}^{I} \sigma_i(x,y) = 1 \quad (2)$$

Woodward et al. (2004) used annual rainfall and the annual minimum of the monthly-mean temperature as the climate controls for vegetation occurrence. Other climate controls can be considered. In this study, we also use annual mean, minimum monthly-mean and maximum monthly-mean rainfall ($R_a$, $R_{min}$ and $R_{max}$, respectively) and temperature ($T_a$, $T_{min}$ and $T_{max}$, respectively) as climate controls. Consequently, nine VC-models with different combinations of rainfall and temperature controls are tested, e.g., $p_i(R_a, T_a)$, $p_i(R_a, T_{min})$ etc.

For today's climate, we use the vegetation-type data with a spatial resolution of 8 km based on remote sensing data from the Advanced Very High Resolution Radiometer (AVHRR, Tucker et al., 2005) and the ERA-Interim (European Centre for Medium Range Weather Forecast Reanalysis – Interim, Dee et al., 2011) data for 1980–2009 to derive the VC-models. The ERA-Interim data (with a resolution of 0.75°) are interpolated to the AVHRR grid for deriving the VC-models. Practically, this is done by sorting vegetation-type data into ($J$, $K$) bins, with bin ($j$, $k$) being defined by ($R_j \pm \mathrm{dR}/2$) and($T_k \pm \mathrm{dT}/2$), such that

$$P_i(R_j, T_k) \equiv p_i(R_j, T_k)\mathrm{dRdT} = N_i(R_j, T_k)/N$$

where $N_i$ is the count of vegetation type $i$ found in bin ($j$, $k$) and $N = \sum_i N_i(R_j, T_k)$ is the sum of $N_i$ over $i$.

To examine the self-consistency of our approach, we applied the VC-models to reconstruct today's vegetation using the ERA-Interim data and compared the reconstruction with the AVHRR vegetation. Fig. 1 shows as example a comparison of the reconstructed map of evergreen broadleaf forest with the corresponding AVHRR map. As seen, the model well reproduced the distribution of this vegetation type, which grows in the warm and humid regions, such as the Amazon, tropical Africa and Southeast Asia (note that the reconstructed map is presented as fraction between 0 and 1, while the AVHRR data is binary 0 or 1). In addition, the Google Earth maps are used for model comparison. The up-to-date Google Earth data have a resolution of 15 m and are independent from the datasets we used for the reconstruction of today's vegetation. A comparison of our maps with the Google Earth maps confirms the good performance of the model.

### 2.2. Goodness of model simulations

To examine the goodness of the VC-models for given vegetation types, we compute for vegetation type $i$ the standard deviation, $D_i$, of

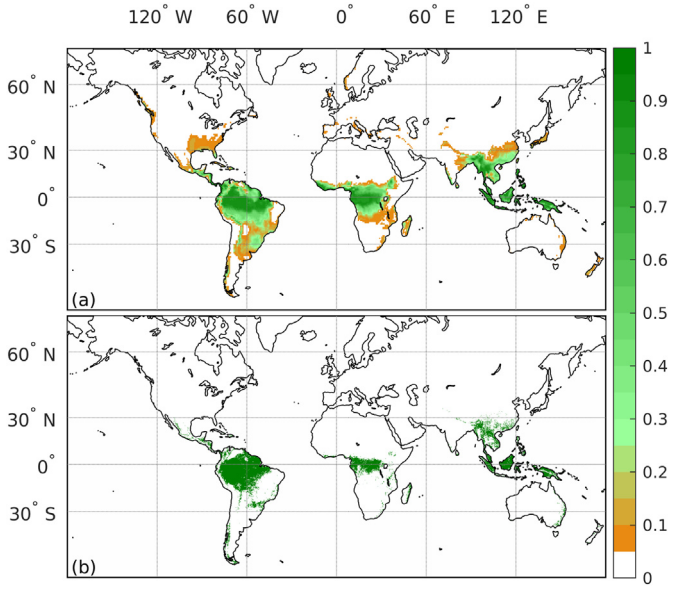


**Fig. 1.** Comparison of (a) reconstructed cover (fraction varying between 0 = 0% and 1 = 100% vegetation cover) of evergreen broadleaf forests for present day based on the ERA-Interim climate using the ($R_a$, $T_a$) model with (b) the corresponding satellite-observed evergreen broadleaf existence (binary: 0 = no evergreen broadleaf forest; 1 = existence of evergreen broadleaf forest) from the AVHRR data.

the difference between the modeled and AVHRR vegetation cover

$$D_i = \frac{1}{L \times M} \sum_{l,m}^{L,M} [\sigma_{im}(l,m) - \sigma_{io}(l,m)]^2 \quad (3a)$$

where $L$ the number of cells in west-east and $M$ that in south-north direction; $\sigma_{im}(l,m)$ is the modeled cover at location ($l$, $m$) of vegetation type $i$, while $\sigma_{io}(l,m)$ the observed by AVHRR. A smaller $D_i$ points to a better performance of the model. As reference, we create a vegetation cover by randomly rearranging the AVHRR data. For the reference case, $D_i$ is maximum

$$D_{i,max} = \frac{1}{L \times M} \sum_{l,m}^{L,M} [\sigma_{im}^2(l,m) - \sigma_{io}^2(l,m)] \quad (3b)$$

Using $D_i$ and $D_{i,max}$, a goodness score is defined

$$S_i = 1 - \frac{D_i}{D_{i,max}} \quad (3c)$$

A perfect simulation has a score one and a random simulation zero. The scores for the 9 VC-models and 11 vegetation types are summarized in Table 1. The VC-models have varying skill in reconstructing the vegetation. For most vegetation types, the reconstruction is much better than the random model, although the score is relatively low for deciduous broadleaf forest. Again, in studying the scores, one needs to keep in mind that the reconstructed map is in fraction between 0 and 1, while the AVHRR data is in binary 0 or 1. The best overall performance is achieved by using the $p_i(R_a, T_a)$ VC-model, with an ensemble score of 0.51. Similar ensemble scores are achieved by using $p_i(R_a, T_{min})$ and $p_i(R_a, T_{max})$. In this study, we present the LGM vegetation reconstructed using the $p_i(R_a, T_a)$ VC-model.

### 2.3. Pollen-based BIOME data

Pollen records have been used for biome reconstructions, a method known as biomisation. Additional information is provided in Supplement S2. The biome classification used in this study follows Harrison (2017), which has 24 classes (Fig. S2). We compressed the 24 classes into 9 M-biome classes for model comparison.

### 2.4. Impact of $CO_2$ concentration on vegetation

Apart from climatic factors, $CO_2$ can influence vegetation patterns, because $CO_2$ affects the water-, light- and nutrient-use efficiencies and hence the photosynthetic rate of plants. In particular, the relative photosynthetic performances of the $C_3$ and $C_4$ plants have been emphasized (Bond et al., 2003). The essential difference between the $C_3$ and $C_4$ modes of photosynthesis is that $CO_2$ partial pressure ($pCO_2$) at the site of Rubisco is 5–10 times higher in the $C_4$ than in the $C_3$ mode. This effectively prevents photorespiration by suppressing $O_2$ competition and saturates Rubisco carboxylase activity. Since photorespiration is temperature and $CO_2$ dependent, photosynthesis is higher in $C_4$ than in $C_3$ plants at higher temperature and lower $pCO_2$. The atmospheric $CO_2$ has been rising from 160 to 200 ppm in the LGM to ~275 ppm in the Holocene and ~407 ppm in 2017. Polley et al. (1993) suggested that the $CO_2$ rise has changed the abundances of $C_3$ plants in Earth's vegetation. Jolly and Haxeltine (1997) suggested that the lower $CO_2$ might explain much of the observed lowering of the montane vegetation belts in East Africa during the LGM. Collatz et al. (1998) reported that $C_4$ plants might have expanded their range substantially during the LGM as a result of the low $CO_2$. Levis et al. (1999) showed reducing $CO_2$ has a significant impact on the modeled vegetation distribution in the tropics and subtropics. Cowling et al. (2001) showed that reducing $CO_2$ to the LGM levels can lead to significantly reduced forest area and density in Amazonia, but lowering temperature can mitigate these changes.

Harrison and Prentice (2003) examined vegetation response to

**Table 1**
Performance scores of the 9 VC-models and 11 vegetation types.

| Model | | 1 | 2 | 3 | 4 | 5 | 6 | 7 | 8 | 9 |
|---|---|---|---|---|---|---|---|---|---|---|
| Climate | Abbr. | $R_{min}$, $T_{min}$ | $R_{min}$, $T_a$ | $R_{min}$, $T_{max}$ | $R_a$, $T_{min}$ | $R_a$, $T_a$ | $R_a$, $T_{max}$ | $R_{max}$, $T_{min}$ | $R_{max}$, $T_a$ | $R_{max}$, $T_{max}$ |
| 1 Evergreen Needleleaf Forest | EN | 0.47 | 0.53 | 0.51 | 0.48 | 0.52 | 0.51 | 0.47 | 0.51 | 0.50 |
| 2 Evergreen Broadleaf Forest | EB | 0.79 | 0.78 | 0.73 | 0.77 | 0.77 | 0.77 | 0.67 | 0.65 | 0.70 |
| 3 Deciduous Needleleaf Forest | DN | 0.23 | 0.40 | 0.25 | 0.38 | 0.41 | 0.27 | 0.42 | 0.41 | 0.28 |
| 4 Deciduous Broadleaf Forest | DB | 0.17 | 0.16 | 0.14 | 0.17 | 0.17 | 0.17 | 0.15 | 0.15 | 0.15 |
| 5 Mixed Forest | MF | 0.32 | 0.34 | 0.29 | 0.30 | 0.34 | 0.31 | 0.30 | 0.31 | 0.31 |
| 6 Woodland | WL | 0.37 | 0.40 | 0.41 | 0.46 | 0.48 | 0.49 | 0.45 | 0.45 | 0.47 |
| 7 Wooded Grassland | WGL | 0.34 | 0.31 | 0.30 | 0.46 | 0.48 | 0.52 | 0.36 | 0.41 | 0.51 |
| 8 Closed Shrubland | CSL | 0.17 | 0.16 | 0.16 | 0.31 | 0.29 | 0.26 | 0.30 | 0.30 | 0.28 |
| 9 Open Shrubland | OSL | 0.40 | 0.37 | 0.31 | 0.51 | 0.50 | 0.45 | 0.48 | 0.49 | 0.47 |
| 10 Grassland | GL | 0.52 | 0.50 | 0.40 | 0.55 | 0.53 | 0.45 | 0.51 | 0.50 | 0.45 |
| 11 Bare Ground | BG | 0.89 | 0.94 | 0.95 | 0.93 | 0.97 | 0.97 | 0.94 | 0.97 | 0.97 |
| 12 Ensemble | | 0.45 | 0.46 | 0.42 | 0.50 | **0.51** | 0.49 | 0.46 | 0.47 | 0.47 |

Bold value represents the largest of the ensemble mean.

climate and $CO_2$ changes between the LGM and today using BIOME4, driven with the data of 17 GCM simulations (see Supplement S3 for more details). The results of Harrison and Prentice (2003) suggest that both $CO_2$ and climate changes are important in determining glacial-interglacial vegetation changes. A common pattern of vegetation distribution is observed in their simulations, e.g., an expansion of treeless vegetation in high northern latitudes; southward displacement and fragmentation of boreal and temperate forests; and an expansion of drought-tolerant biomes in the tropics. Harrison and Prentice (2003) found that global forest cover was overestimated by all models if climate change alone was used to drive BIOME4, but better estimated when the $CO_2$ effects were included. The low $CO_2$ during the LGM restricted the extent of forests, especially in the tropics where forests lost ground to grasses, shrubs and savannas. These features appear to be broadly consistent with pollen-based vegetation reconstructions, but contradictory evidence also seems to exist (Haberle and Maslin, 1999).

Major $C_3/C_4$ ecosystems include savannas in which $C_3$ trees coexist with $C_4$ herbaceous plants, and grasslands in which $C_3$ grasses coexist with $C_4$ herbaceous plants. $C_3/C_4$ savannas occur in relatively hot, humid or sub-humid climates (e.g. tropical Africa), while $C_3/C_4$ grasslands occur in temperate or subtropical climates with humid to sub-humid conditions (e.g. North America). Although the $C_4$ flora comprises a relatively small number of species, $C_3/C_4$ ecosystems constitute a large part of global vegetation (Lattanzi, 2010).

However, the vegetation shift in response to climate and $CO_2$ is very complex. Izumi and Lézine (2016) examined the vegetation response to $CO_2$ using pollen-based reconstructions over the past 18,000 years at two equatorial mountain sites (Bambili, 5°56′N and 10°14′E; Rusaka, 3°26′S and 29°37′E). The two sites have similar altitude and approximately the same vegetation distribution during the LGM. It is found that vegetation change was more pronounced in Rusaka (where it had somewhat more grass/shrubs during the LGM) than in Bambili (where it had somewhat more forest) in all periods. The simulated NPP for the various biomes at the two sites using BIOME4 and BIOME5-beta, driven with the same climate data, revealed opposing responses between the models, indicating that the models need to be re-evaluated to produce robust results. Wu et al. (2007) pointed out that whether the vegetation prior to the Holocene is due to lower $CO_2$, change in climate or their combination is still an unresolved question.

The above discussion suggests that, despite of uncertainties, the VC-model is likely a function of $CO_2$, as Fig. 2 illustrates. We thus rewrite Eq. (1) as

$$P_i(x,y) = \int p_i[R(x,y), T(x,y); C]\,\mathrm{dRdT} \tag{1a}$$

with $C$ being a parameter representing $CO_2$ in the VC-model,

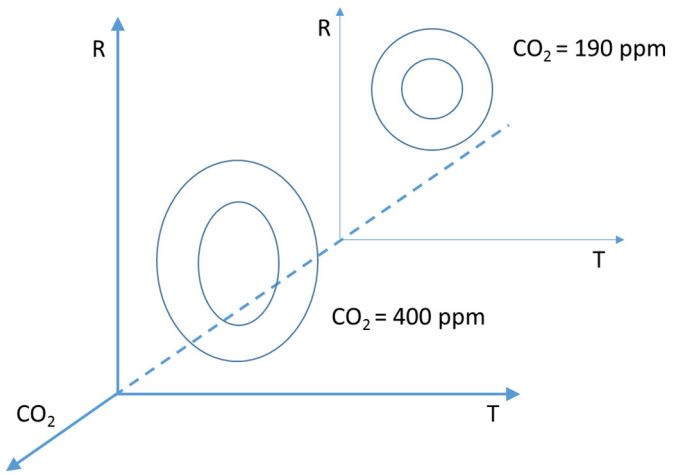


**Fig. 2.** Schematic illustration of transition of vegetation probability (contours) as function of temperature, $T$, and rainfall, $R$, for different $CO_2$.

**Table 2**
Transition factors for the vegetation biome based on Woillez et al. (2011) for LGM climate with $CO_2$ = 310 ppm and 180 ppm. Transition factor is the ratio of the fraction cover at $CO_2$ = 180 ppm/fraction cover at $CO_2$ = 310 ppm.

| Vegetation class | Transition factor |
|---|---|
| Evergreen Needleleaf Forest | 0.28 |
| Evergreen Broadleaf Forest | 0.73 |
| Deciduous Needleleaf Forest | 0.2 |
| Deciduous Broadleaf Forest | 0.76 |
| Mixed Forest | 1.0 |
| Woodland | 1.62 |
| Wooded Grassland | 1.62 |
| Closed Shrubland | 1.66 |
| Open Shrubland | 1.66 |
| Grassland | 1.69 |
| Bare Ground | 1.15 |

$p_i(R,T;C)$. Our task is now to map the VC-model from today's $CO_2$ level to the LGM $CO_2$ level. A simple model conceivable is

$$p_i(R,T;C) = \sum_j m_{ij}(C)p_j(R,T) \tag{4}$$

constrained by the condition that the transition matrix $|m_{ij}| = 1$. Although $m_{ij}$ in reality may be complex in detail, it is likely to be a sparse matrix. The simplest is that $m_{ij}$ is diagonal.

We estimate the transition matrix from the results of Woillez et al. (2011), who used a dynamical global vegetation model, driven with the outputs of a GCM and run for the LGM and modern $CO_2$ levels, to assess the impacts of the changes in climate and $CO_2$ on vegetation. Woillez et al. (2011) showed that their model correctly reproduced the broad features of the glacial vegetation reconstructed from pollen data for the LGM. Table S3.3 and S3.4 show the cover fraction of the plant functional types, as well as $C_3$, $C_4$ and bare soil, in the tropical, temperate and boreal environments. Based on the results, the transition factors are estimated as listed in Table 2. We used the transition coefficients in Table 2 to correct the effect of $CO_2$ on the reconstructed LGM vegetation cover using the VC-model.

Today's vegetation is subjected to a rapidly increasing $CO_2$, so it may be that today's vegetation response to $CO_2$ is unsteady. Therefore, it is appropriate to ask whether the unsteadiness may lead to bias in the $CO_2$ corrections. An examination of the global annual mean NDVI (Normalized Differential Vegetation Index) for 1982–2016 reveals that its increase has been insignificant in this period during which $CO_2$ elevated from ~350 ppm to ~400 ppm. Even if an increase in NDVI can be detected, it is hard to tell whether it is due to the global warming or to the $CO_2$ increase. Thus, the effect of the recent $CO_2$ increase on today's vegetation is not profound and the $CO_2$ corrections listed in Table 2 are not strongly affected by the unsteadiness of the $CO_2$ in today's climate.

### 2.5. Ensemble average of model-simulated LGM climate

As climate control we use the monthly averages from the PMIP3 21 ka CGCM/ESM simulations. The monthly rainfall and temperature averages are ensemble-averaged over six GCMs listed in Table 3. The simulations were made following the PMIP3 21 ka experimental design, including the blended ice sheet data by ICE-6G (Peltier et al., 2015), Australian National University (ANU) Ice Model (Lambeck and Chappell, 2001; Lambeck et al., 2002), and GLAC-1 (Tarasov and Peltier, 2002, 2003). Model skill has been assessed for some members by comparing the pre-industrial runs with the NCEP/NCAR Reanalysis (Kalnay et al., 1996), for example, in Ludwig et al. (2016).

The simulated data of the selected CGCM/ESM are first interpolated to a grid of 0.75° × 0.75° of horizontal resolution on the ERA-Interim grid and then ensemble averaged to obtain the mean climate controls.

**Table 3**
List of models participating in PMIP3 and used in this study to generate the ensemble averages of the LGM climate from the selected model years. The ensemble codes (r: realization, i: initialization, p: physics) and key-references are also listed.

| Model | Model years | Ensemble code | Reference |
|---|---|---|---|
| CNRM-CM5 | 1800–1999 | r1i1p1 | Voldoire et al. (2013) |
| FGOALS-g2 | 0550–0649 | r1i1p1 | Bao et al. (2013) |
| IPSL-CM5A-LR | 2601–2800 | r1i1p1 | Kageyama et al. (2013) |
| MIROC-ESM | 4600–4699 | r1i1p1 | Sueyoshi et al. (2013) |
| MPI-ESM-P | 1850–1949 | r1i1p1 | Giorgetta et al. (2013) |
| MRI-CGCM3 | 2501–2600 | r1i1p1 | Yukimoto et al. (2012) |

Fig. 3 compares the (ensemble averaged) annual mean precipitation and annual mean temperature for the simulated LGM climate and the todays ERA-Interim climate.

Based on the ensemble mean data, the temperature over the ice sheets was lower by 20 to 30 K (e.g. Laurentide Ice Sheet, North America). The simulated temperature differences are in line with the proxy-based reconstructions (Bartlein et al., 2011): relatively large temperature differences (> 8 °C) are found close to the northern-hemisphere ice sheets and small differences (< 3 °C) in the tropics. Likewise, the features of the annual mean precipitation, e.g., a decrease in central Africa (Bartlein et al., 2011), an increase/decrease in western/eastern North America (Bartlein et al., 2011; Oster et al., 2015), a general decrease in Amazonia and an increase in northeastern Brazil (Wainer et al., 2005) are consistent with the proxy data.

At lower latitudes, temperature was a few degrees lower than today. According to the PMIP3 simulations, precipitation was reduced in today's regions of heavy rainfall, such as the Amazon and the South Atlantic Convergence Zone, as well as the monsoon affected areas, such as East Asian monsoon area, the Indian monsoon area. Much of the earth was drier during the LGM, but today's desert areas generally received somewhat more rain (likely due to inadequate treatment of drizzle in the GCMs/ESMs).

## 3. Results

Using the techniques and data described in Section 2, the VC-models are derived for today's climate and $CO_2$. Fig. 4a, b and c show $P_i$ for all vegetation types as function of monthly-averaged precipitation and monthly-averaged temperature. It is seen in Fig. 4a, for example, that evergreen needleleaf forest exists in a cooler and drier climate than evergreen broadleaf forest, and they co-exist under certain climate conditions (e.g. $R_a$ = 10 mm/day and $T_a$ = 283 K); bare ground exists in hot-and-dry climate, as well as in cold-and-dry and cold-and-humid climate; open shrubland and bare ground co-exist under hot and dry climate conditions.

The probabilities with $CO_2$ corrections (from today's $CO_2$ to $CO_2$ = 185 ppm in LGM, see Section 2.4) are shown in Fig. 4d, e and f. The basic features of the probabilities with or without $CO_2$ corrections are similar, but quantitative differences are visible, for example, in the reduced probability of evergreen broadleaf and evergreen needleleaf forests. Also the probability of deciduous needleleaf forests is reduced, while that of grassland increased.

Using the simulated climate data for the LGM (Section 2.5), the model produced very different vegetation covers between the LGM and today. Fig. 5 shows as example the reconstructed fraction of vegetation cover of grassland, open shrubland, evergreen needleleaf forest and bare ground, together with the vegetation density differences between the LGM and today (see Supplement S4 for other vegetation types). These results are obtained with $CO_2$ corrections and represent both the effect of climate and $CO_2$ changes on vegetation. In comparison with today, there was less grassland at high latitudes due to reduced temperature and rainfall, but more grassland in today's desert areas, such as the Sahara, the Middle East and central Australia. In these areas, due to the lower temperature and hence reduced potential evaporation, grassland could survive despite of the low rainfall in the LGM. In

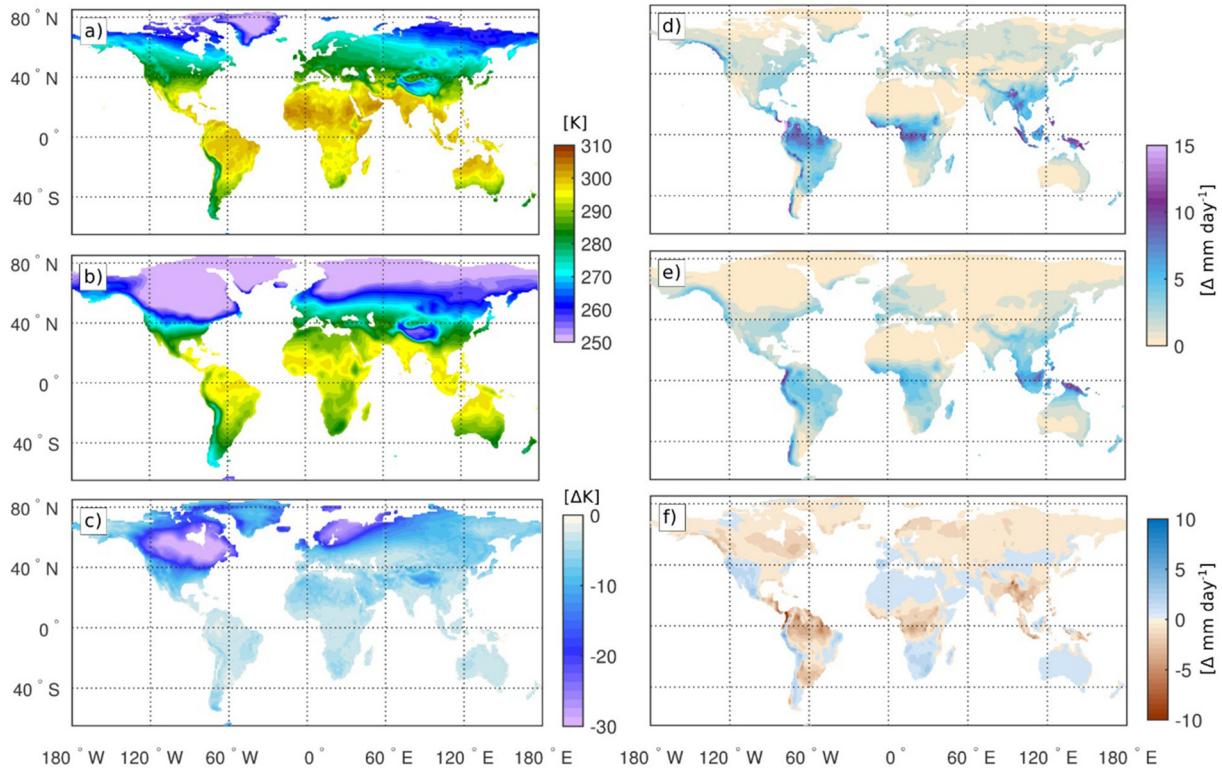


**Fig. 3.** (a) Annual mean temperature of ERA-Interim; (b) Annual mean temperature of PMIP3 ensemble for LGM; (c) temperature difference between LGM and ERA-Interim; (d), (e) and (f), as (a), (b) and (c), but for daily precipitation rate.

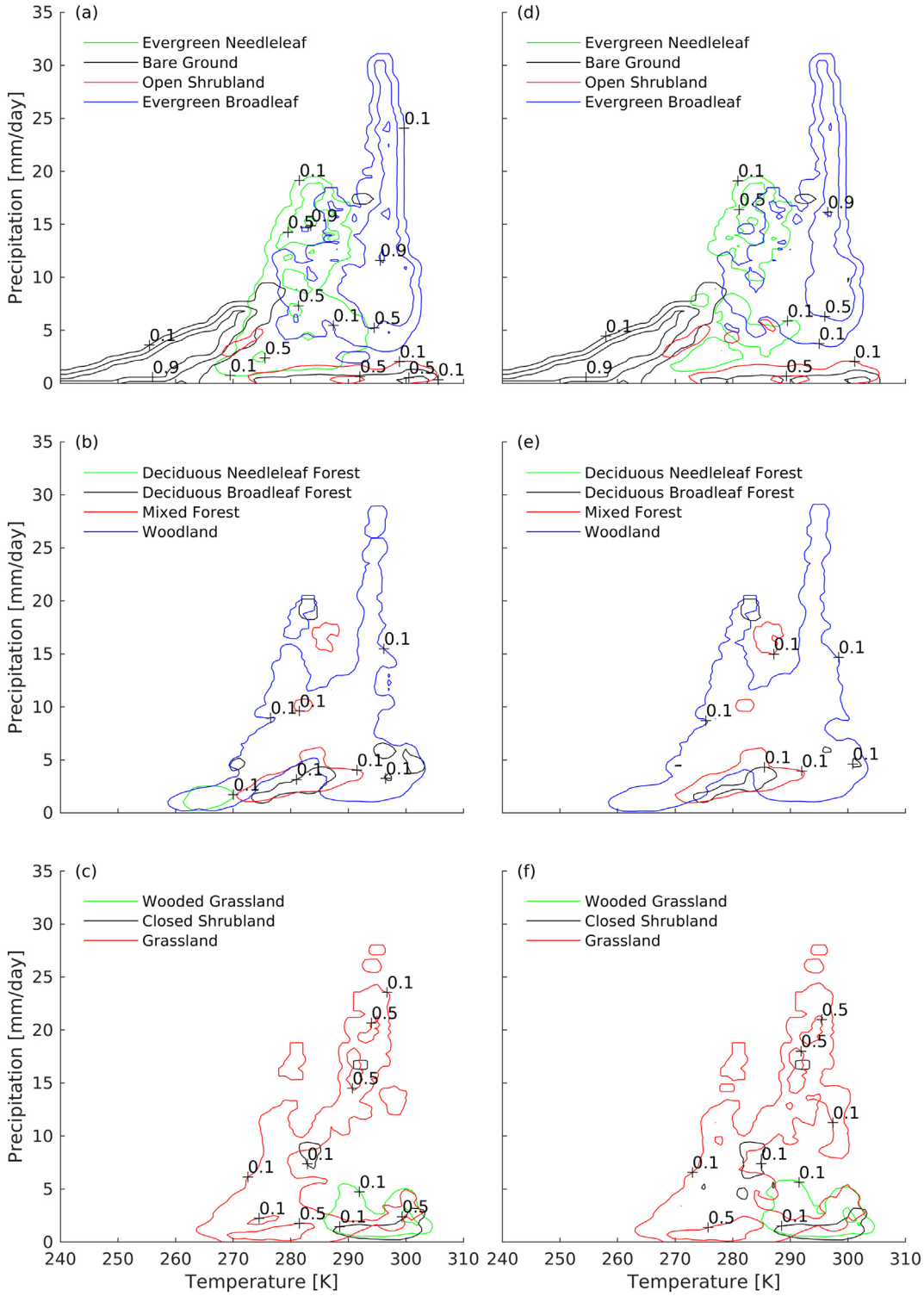


**Fig. 4.** Probabilities $P_i$ for 11 vegetation types, (a), (b) and (c), as function of mean monthly-averaged precipitation and mean monthly-averaged temperature estimated using the AVHRR vegetation cover data and ERA-Interim data for 1980–2009. The probabilities with $CO_2$ corrections corresponding to (a), (b) and (c) are shown in (d), (e) and (f).

similarly dry and cold regimes of today's climate, grassland exists, for instance, in the arid regions of the temperate grassland. Accompanying these changes in grassland, there was much less needleleaf forest at high latitudes, although slightly more in some areas at the middle and low latitudes. For example, the reconstruction suggests that in southern Africa, covered today mainly by woodland, a low-density needleleaf forest was possible during the LGM. Due to the cold climatic conditions, much of the high latitudes in the Northern Hemisphere were bare ground, covered either by ice or undefined land surface types (areas with climate conditions that do not exist today, e.g. a region colder than any region on today's planet). In the Sahel, today's open shrubland was replaced by woodland in the LGM, while the northern part of the Sahara, the fraction of open shrubland increased by about 30%. This suggests that in terms of vegetation, the southward extent of the Sahara

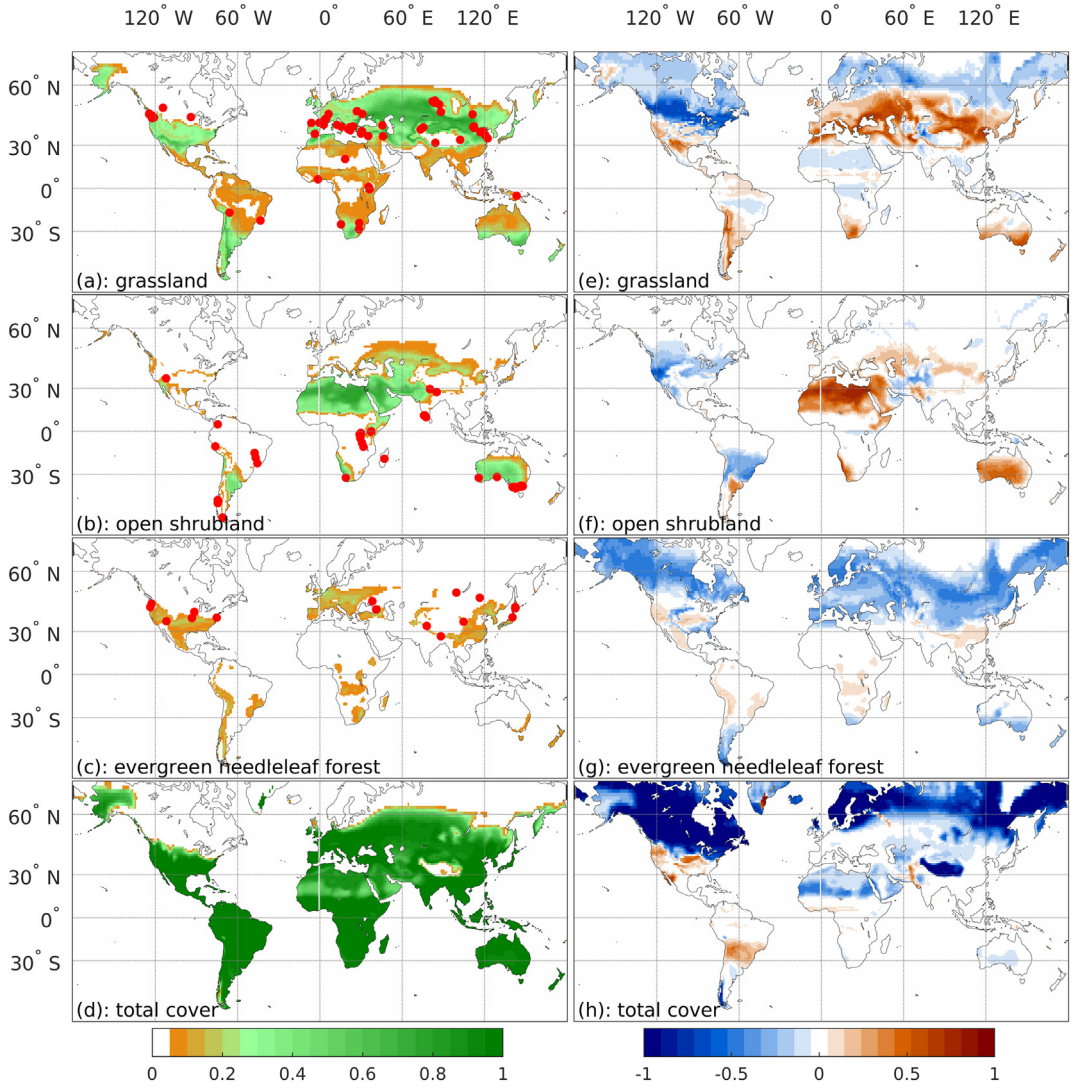


**Fig. 5.** Reconstructed vegetation density, with $CO_2$ correction, for (a) grassland, (b) open shrubland, (c) needleleaf forest and (d) fraction of cover (1 - bare ground) for the LGM and the corresponding vegetation density differences between the LGM and today (LGM minus today) shown in (e) to (h). The red dots in (a), (b) and (c) mark the locations of the corresponding BIOME-6000 data (Harrison, 2017 and reference therein). (For interpretation of the references to colour in this figure legend, the reader is referred to the web version of this article.)

desert was reduced in the LGM climate. Consistent with this finding is that the bare soil fraction was reduced in North Africa, as seen in Fig. 5d and h.

The vegetation patterns reconstructed with and without $CO_2$ corrections are compared (not shown). It is found that while the global vegetation patterns, reconstructed with and without $CO_2$ corrections, are largely similar, noticeable regional differences can be identified. For example, with $CO_2$ correction, in the tropics, the reduction of grassland at Northern Hemisphere high latitudes remains unchanged, but the increase at mid/low latitudes is more pronounced. Also, the strong reduction of evergreen needleleaf forest at Northern Hemisphere high latitudes remains unchanged, but the increase at mid/low latitudes due to the effect of climate is moderated by the lower $CO_2$.

Pollen data have been used to reconstruct paleo-climate variables for certain locations (Simonis et al., 2012) and on global scales (Bartlein et al., 2011), which can be used for the evaluation of paleo-climate model simulations (Harrison et al., 2014). In the BIOME-6000 (Prentice and Webb III, 1998; Prentice et al., 2000), a global biome database has been compiled for the periods of the LGM, mid-Holocene and present-day. In that project, pollen and plant-macro-fossil sources dated to the LGM are used to estimate the vegetation species, which are then reclassified as biomes. The BIOME-6000 biome data has been updated many times (Prentice et al., 2000; Bigelow et al., 2003; Pickett et al., 2004; Marchant et al., 2009; Harrison and Bartlein, 2012). Harrison (2017) converted the original nomenclature from the various regions in the BIOME-6000 database to a standardized classification. This dataset (see http://researchdata.reading.ac.uk/99/) is used for comparison with our reconstructions (Fig. 5 and Fig. S4.1, S4.2). While biome data for the LGM are rather sparse, consistency can be found between the model-reconstructed and polled-based biomes. The reconstructed grassland zones in the LGM are largely confirmed by the pollen-based estimates. Again, it should be mentioned that with the present model, no statement on the vegetation types in LGM can be made, which do not occur in today's climate. Some inconsistencies are found in the comparisons between the reconstructed vegetation of needleleaf forest (Fig. 5c), mixed forest (Fig. S4.2d) and woodland (Fig. S4.2e) and the pollen-based biomes. For example, pollen-based biomes suggest the existence of needleleaf forest near Lake Baikal, but our reconstruction not. This indicates that the GCM simulated climate may be colder here than it was in reality. More work is needed to reconcile the difference between the model-reconstructed and polled-based biomes.

The global areal coverage of the vegetation in today's and LGM's

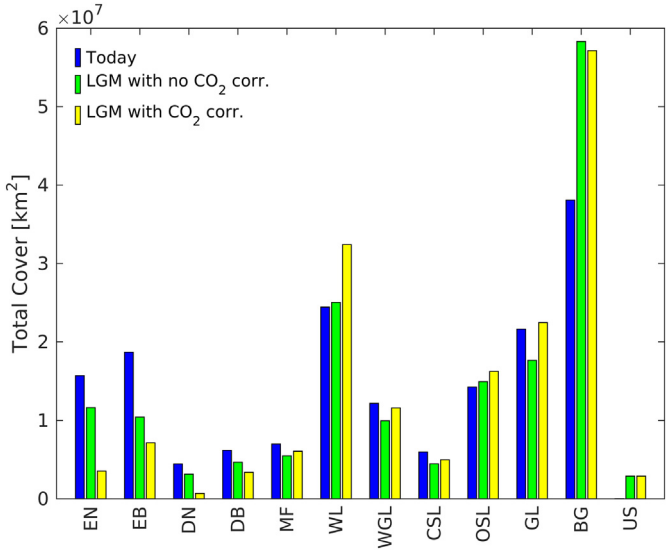


**Fig. 6.** Global areal coverage by various biomes in today's climate based on satellite data and reconstructed for the LGM with and without $CO_2$ corrections. See Table 1 for abbreviation of vegetation types.

climate, with and without $CO_2$ corrections, are shown in Fig. 6. Due to the existence of ice sheet and extended cold deserts, there existed less vegetation and much (about 1/3) more bare ground in the LGM compared to today. Apart from grassland and mixed forest, the amount of all other vegetation types were reduced due to the colder and drier climate in the LGM. Evergreen broadleaf forest underwent the strongest reduction with the area shrunk by more than a half. The $CO_2$ correction resulted in further reductions of the forested areas, but moderated the reduction of wood-, shrub- and grasslands.

The Amazon and Sahara stand out as two regions with profound changes in vegetation. Today's Amazon is basically covered by evergreen broadleaf forests in the central area and woodland at its fringes as shown in Fig. 7a and b (note that the analysis of vegetation in the Amazon, we used all data in the region shown in Fig. 7a, not the Amazon hydrological basin). Vegetation evolution in the Amazon for the present (Davidson et al., 2012) and in the past (Wang et al., 2017) is of great interest. During the LGM, the coverage of the rainforest shrunk considerably both in area and density. For example, under today's condition, the center of the Amazon has a cover of evergreen broadleaf forest of > 80%, and the southern fringes of 30 to 40%. Under the LGM conditions, the cover was reduced to ~40% in central Amazon due to climate change, and the lower $CO_2$ further enhanced the reduction to below 40% (Fig. 7c). During the LGM, the rainforest of the Amazon was more confined (~1/3 of today's cover), replaced by more widely spread woodland (Fig. 7f), wooded grassland and grassland (Fig. 7g). The vegetation density function for the Amazon under today's and the LGM climate conditions is shown in Fig. S5.1a (with no $CO_2$ correction) and S5.2a (with $CO_2$ correction). Under today's climate, the Amazon is dominated by evergreen broadleaf forest and woodland with some probabilities of deciduous broadleaf, wooded grassland and grassland. During the LGM, the ensemble mean climate in the Amazon was cooler (mean monthly-averaged temperature decreased by 2–4 °C for the LGM conditions) and drier (mean monthly rainfall down from about 10 mm/day today to 6 mm/day). This corresponds well with the proxy data reconstructions of temperature and precipitation in this region (Stute et al., 1995; Wainer et al., 2005; Annan et al., 2013; Wang et al., 2017). The Amazon climate during the LGM was similar to the climate of Southwest China today and consequently, the vegetation was a more complex mixture of evergreen broadleaf, woodland, mixed forest, wooded grassland, grassland as well as evergreen needleleaf and deciduous broadleaf forests (Fig. 7g).

Today, the Saharan desert dominates Northern Africa's landscape, predominantly by some open shrubland and grassland, as shown in Fig. 8a and b (again, for the analysis of vegetation in Sahara, we used all data in the region shown in Fig. 8a, not the Sahara Desert). This is determined by the extreme arid conditions of high temperature and low rainfall in the Sahara and the monsoon rainfall in the Sahel. The reconstructed vegetation suggests that during the LGM, the Sahara was more vegetated than today: it was covered by up to 40% open shrubland and 40% grassland (Fig. 8c and d). Reduced $CO_2$ in LGM further increased the cover of open shrubland and grassland (Fig. 8g). The fraction of bare ground in large areas of the Sahara was reduced from today's 80% to about 20 to 30%. The Sahel was also much more covered by open shrubland and, to some degree, closed shrubland. The vegetation density function for North Africa under today's and the LGM climate conditions is shown in Fig. S5.1b (with no $CO_2$ correction) and S5.2b (with $CO_2$ correction). In the LGM, the climate of North Africa was cooler (temperature lower by 10 K) and somewhat more humid (rainfall between 0.1 and 0.7 mm/day). While the precipitation was still very low, but due to the significantly reduced temperature and hence potential evaporation, the presence of grassland and open shrubland over large areas of North Africa was possible.

The conclusion based on the reconstruction that the Sahara had significant vegetation cover is disputable. Questions arise whether this result is due to a model bias in rainfall over-prediction in the desert areas (e.g. too much drizzle). To check this, we conduct sensitivity tests on the reconstructed vegetation in the Sahara on rainfall. Vegetation density for the Sahara is reconstructed by reducing the rainfall by 10, 20 and 30%. However, the results are basically the same. Studies have shown that the climate of the Sahara is characterized by orbital-scale variations of the North African Monsoon. During periods of strong monsoon, precipitation and vegetation in the Sahara increase, causing a “Green Sahara”. During periods of weak monsoon, precipitation and vegetation in the Sahara decrease, causing a “Desert Sahara”. The cyclic variations in the Saharan climate has been largely attributed to the changes in insolation related to the earth's orbital parameters. Kutzbach (1981) hypothesized that orbital-scale changes of insolation may be the underlying driver of the monsoon cycles. Claussen et al. (2002) and Tjallingii et al. (2008) found that enhanced summer monsoon led to a humid Sahara during the Holocene until ~5 ka BP. Larrasoaña et al. (2013) showed that over the past 8 Ma “Green Sahara” frequently occurred. Based on the results shown in Fig. 8, we speculate that in terms of vegetation density, a different “Green Sahara” could come to existence not due to enhanced summer monsoon but reduced evaporation. While this speculation cannot at this stage be rigorously verified, it is consistent with the Oxford Lake-Level Data Base (Street-Perrott et al., 1989) for records of changes in lake status (e.g. relative water depth). The lake status data for 18 ka BP indicate a higher value of net water influx (precipitation minus evaporation) for North Africa. Thus, a larger potential for humidity-limited vegetation was not impossible. Also, our speculation does not contradict the findings of Dupont (2011) who presented marine sediment records of pollen along the eastern coast of Africa. The pollen data appear to indicate more frequent Poaceae (representative for Savannah) and Asteraceae (representative for semi-desert) during the glacial than during interglacial times.

## 4. Concluding remarks

e used a simple statistical approach to reconstruct the global vegetation cover for the LGM. Following the IGBP vegetation classification, we divided the land cover into 11 vegetation types plus bare soil. For each of them, we derived a statistical relationship between the probability of its occurrence and climate variables, referred to as the VC-models. The statistical relationships are then $CO_2$ corrected. Using these VC-models without and with $CO_2$ corrections, we reconstructed the vegetation densities under LGM climate conditions.

In deriving the VC-models, the AVHRR vegetation data and the

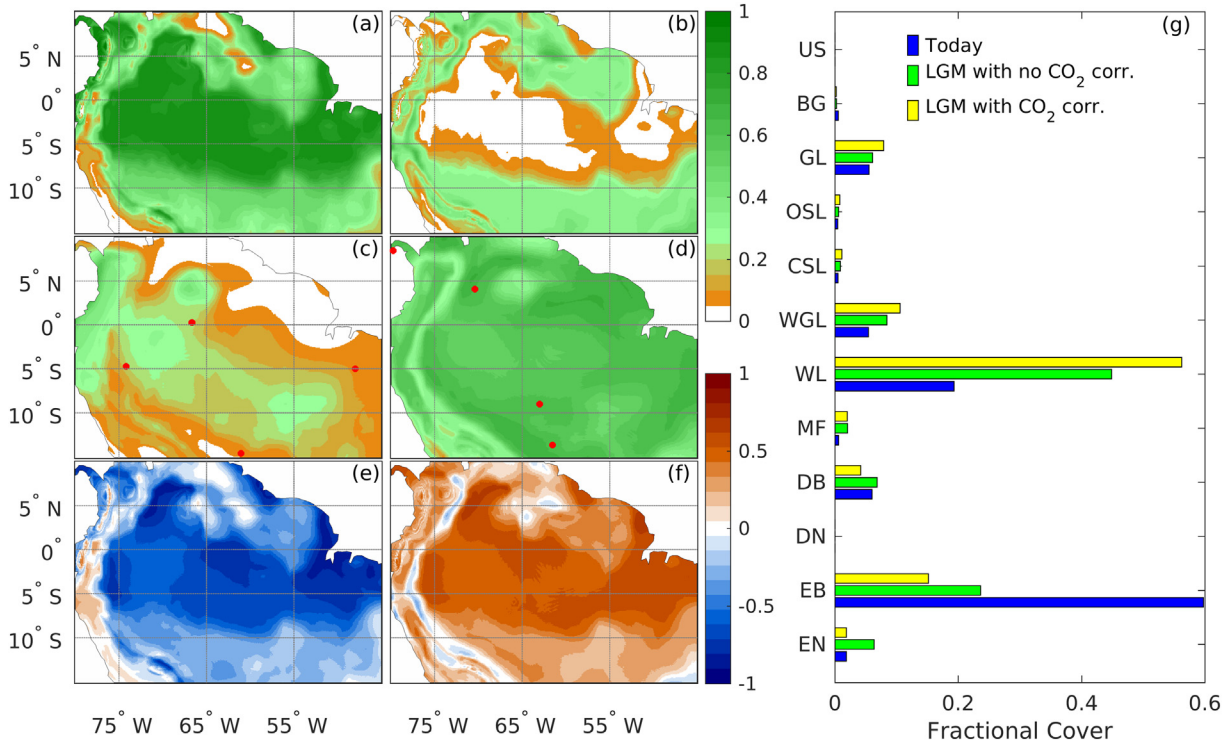


**Fig. 7.** Density of the two main vegetation types in the Amazon for today's climate (a) evergreen broadleaf forests and (b) woodland; (c) and (d), as (a) and (b), but for the LGM with $CO_2$ correction; The red dots in (c) and (d) mark the locations of the corresponding BIOME-6000 data (Harrison, 2017 and reference therein); (e) and (f), respectively differences in evergreen broadleaf forests and woodland between the LGM and today (LGM – today); (g) fraction of vegetation cover for today's climate, for the LGM with no $CO_2$ correction and with $CO_2$ correction. See Table 1 for abbreviation of vegetation types. (For interpretation of the references to colour in this figure legend, the reader is referred to the web version of this article.)

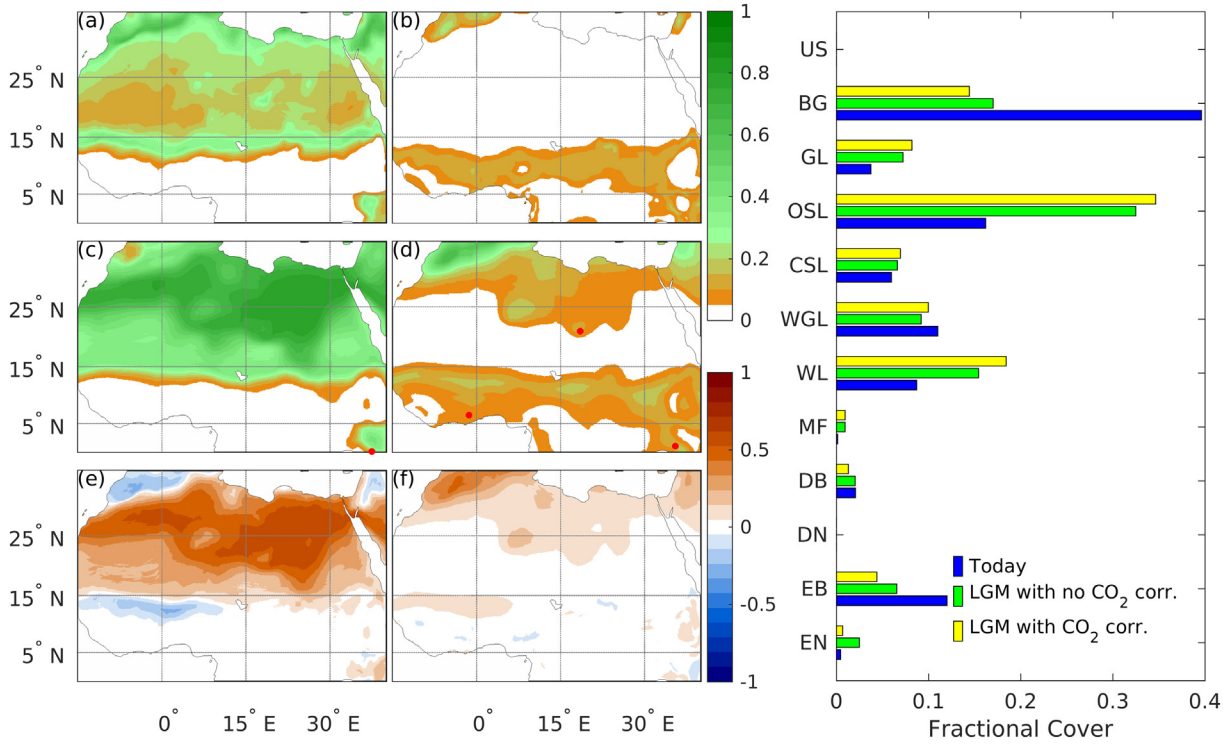


**Fig. 8.** Density of the two main vegetation types in North Africa for today's climate (a) open shrubland and (b) grassland; (c) and (d), as (a) and (b), but for the LGM with $CO_2$ correction; The red dots in (d) mark the locations of the corresponding BIOME-6000 data (Harrison, 2017 and reference therein). (e) and (f), differences in open shrubland and grassland between the LGM and today (LGM – today); (g) fraction of vegetation cover for today's climate, the LGM with no $CO_2$ correction and with $CO_2$ correction. See Table 1 for abbreviation of vegetation types. (For interpretation of the references to colour in this figure legend, the reader is referred to the web version of this article.)

ERA-Interim reanalysis data are used. Nine different VC-models were tested by reconstructing today vegetation using the ERA-Interim data and comparing the reconstructions with the observations. Among the models tested, the VC-models using monthly mean rainfall and monthly mean temperature as climate drivers give the best overall performance.

For the LGM, climate data were taken from an ensemble mean of PMIP3 global climate model simulations. Compared to today's climate, the LGM climate was in general colder and drier and $CO_2$ was much lower. The different climate and $CO_2$ conditions resulted in profoundly different vegetation cover in the LGM, as already known from many previous studies. However, climate change contributed to about 75% of the variance in the vegetation difference between the LGM and today, while $CO_2$ change 25%. For certain vegetation types, the climate impact is strengthened by and $CO_2$ effect, e.g. increased grassland and decreased evergreen broadleaf forest in the LGM, while for others, the climate impact is moderated by the $CO_2$ effect, e.g. increased needle leaf forest in the mid/low latitudes due to climate change is moderated by the low $CO_2$ in the LGM. From the global perspective, in the LGM, there was less vegetation due to extended ice sheets and cold deserts and much of the high latitudes was bare. The vegetation regimes of today were shifted to cooler and drier vegetation regimes in the LGM. For example, in the Northern Hemisphere, there was less grassland at high latitudes. In today's desert areas, however, including the Sahara, the Middle East and central Australia, due to reduced temperature and increased precipitation, the vegetation cover possibly increased during the LGM. Accompanying the changes in grassland, there were less needleleaf forests at high latitudes but more at the mid/ low latitudes. The climate impact and $CO_2$ effect combined resulted in a significant shrinkage of forest areas, especially in the tropics. The reconstructed vegetation cover is generally supported by the pollen data.

The Sahara and the Amazon experienced profound changes in vegetation. While evergreen broadleaf forests in its center and woodland at its fringes cover today's Amazon, both their coverage area and density were significantly smaller during the LGM. > 80% of today's central Amazon and 30 to 40% of its southern fringes are covered by evergreen broadleaf forest. During the LGM, rainforest cover reduced to < 40% in central Amazon, and completely disappeared at the fringes, replaced by needle-leaf forests, mixed forests and woodlands. While today's North Africa comprises mainly the bare ground of the Sahara and shrubland and wooded grassland of the Sahel, in the LGM, the Sahara was more vegetated, covered by up to 35% shrubland and 35% grassland and the bare ground fraction reduced from today's 80% to 30%. The Sahel was more covered by grassland and open shrubland.

Our vegetation cover reconstruction relies on the reliability of the PMIP3 simulations. An important implication of our model results is that the global vegetation cover and density for the LGM probably differs substantially from what is specified in the GCM/EMS simulations. Numerical experiments are being planned to examine how the changed vegetation cover and density influence model results both on global and regional scale. We expect that some iterations will be required to reach a steady state vegetation distribution.

## Author contribution statement

Yaping Shao designed the work, developed the methodology and wrote the paper; Andreas Anhäuser initiated the work and carried out preliminary tests; Patrick Ludwig prepared and analyzed the paleoclimate data; Philipp Schlüter prepared the software, carried out data analysis and prepared all the graphs except Fig. S1; Ehimen Williams collected the biome data for comparison with the reconstructed vegetation. All authors reviewed the manuscript.

## Additional information

There is no competing interests.

## Acknowledgement

This work is supported by the DFG Collaborative Research Center 806 “Our Way to Europe”. The reconstructed data are available from the public data repository http://dx.doi.org/10.17632/cr269zdybh.1 (Shao et al., 2018). Unless specifically stated, the graphs are generated using NCL (NCAR Command Language, http://www.ncl.ncar.edu).

## Appendix A. Supplementary data

Supplementary data to this article can be found online at https://doi.org/10.1016/j.gloplacha.2018.06.002.

## References

Annan, J.D., Hargreaves, J.C., et al., 2013. Clim. Past 9, 367–376. http://dx.doi.org/10.5194/cp-9-367-2013.
Bao, Q., et al., 2013. The flexible global ocean-atmosphere-land system model, spectral version 2: FGOALS-s2. Adv. Atmos. Sci. **30**, 561–576. http://dx.doi.org/10.1007/s00376-012-2113-9.
Bartlein, P.J., et al., 2011. Pollen-based continental climate reconstructions at 6 and 21 ka: a global synthesis. Clim. Dyn. 37, 775–802. http://dx.doi.org/10.1007/s00382-010-0904-1.
Bigelow, N.H., et al., 2003. Climate change and arctic ecosystems: 1. Vegetation changes north of 55 N between the last glacial maximum, mid-Holocene, and present. J. Geophys. Res. **108** (D19), 8170. http://dx.doi.org/10.1029/2002JD002558.
Binney, H., et al., 2016. Vegetation of Eurasia from the last glacial maximum to present: key biogeographic patterns. Quat. Sci. Rev. **157**, 80–97. http://dx.doi.org/10.1016/j.quascirev.2016.11.022.
Bond, W.J., Midgley, G.F., Woodward, F.I., 2003. The importance of low atmospheric CO2 and fire in promoting the spread of grasslands and savannas. Glob. Change Biol. 9, 973–982. http://dx.doi.org/10.1046/j.1365-2486.2003.00577.x.
Braconnot, P., et al., 2012. Evaluation of climate models using palaeoclimatic data. Nat. Clim. Chang. 2, 417–424. http://dx.doi.org/10.1038/nclimate1456.
Clark, P.U., et al., 2009. The last glacial maximum. Science 325, 710–714. http://dx.doi.org/10.1126/science.1172873.
Claussen, M., Brovkin, V., Ganopolski, A., 2002. Africa: Greening of the Sahara. In: Steffen, W., Jäger, J., Carson, D.J., Bradshaw, C. (Eds.), Challenges of a Changing Earth. Global Change — The IGBP Series. Springer, Berlin, Heidelberg, pp. 125–128. http://dx.doi.org/10.1007/978-3-642-19016-2_23.
CLIMAP Project Members, 1984. The last interglacial ocean. Quat. Res. **21**, 123–224. http://dx.doi.org/10.1016/0033-5894(84)90098-X.
Collatz, G.J., Berry, J.A., Clark, J.S., 1998. Effects of climate and atmospheric CO2 partial pressure on the global distribution of C 4 grasses: present, past, and future. Oecologia 114, 441–454. http://dx.doi.org/10.1007/s004420050468.
Cowling, S.A., Maslin, M.A., Sykes, M.T., 2001. Paleovegetation simulations of Lowland Amazonia and implications for neotropical allopatry and speciation. Quat. Res. **55**, 140–149. http://dx.doi.org/10.1006/qres.2000.2197.
Davidson, E.A., et al., 2012. The Amazon basin in transition. Nature 481, 321–328. http://dx.doi.org/10.1038/nature10717.
Dee, D.P., et al., 2011. The ERA-interim reanalysis: configuration and performance of the data assimilation system. Quat. J. Royal Meteorol. Soc. 137, 553–597. http://dx.doi.org/10.1002/qj.828.
Dickinson, R.E., et al., 2006. The community land model and its climate statistics as a component of the community climate system model. J. Clim. 19, 2302–2324. http://dx.doi.org/10.1175/JCL13742.1.
Dupont, L.M., 2011. Orbital scale vegetation change in Africa. Quaternary Science Reviews 30, 3589–3602. http://dx.doi.org/10.1016/j.quascirev.2011.09.019.
Giorgetta, M.A., et al., 2013. Climate and carbon cycle changes from 1850 to 2100 in MPI-ESM simulations for the coupled model Intercomparison project phase 5. J. Adv. Model. Earth Syst. 5, 572–597. http://dx.doi.org/10.1002/jame.20038.
Guiot, J., et al., 1999. The climate of the Mediterranean Basin and of Eurasia of the last glacial maximum as reconstructed by inverse vegetation modelling and pollen data. Ecol Medit 25, 193–204.
Haberle, S., Maslin, M., 1999. Late quaternary vegetation and climate change in the Amazon Basin based on a 50,000 year pollen record from the Amazon fan, ODP site 932. Quat. Res. 51 (1), 27–38. http://dx.doi.org/10.1006/qres.1998.2020.
Harrison, S., 2017. BIOME 6000 DB classified plotfile version 1. http://researchdata.reading.ac.uk/99.
Harrison, S.P., Bartlein, P., 2012. Records from the past, lessons for the future: what the palaeorecord implies about mechanisms of global change. http://hdl.handle.net/1959.14/195862.
Harrison, S.P., Prentice, C.I., 2003. Climate and CO2 controls on global vegetation distribution at the last glacial maximum: analysis based on palaeovegetation data, biome modelling and palaeoclimate simulations. Glob. Change Biol. 9, 983–1004. http://dx.doi.org/10.1046/j.1365-2486.2003.00640.x.
Harrison, S.P., et al., 2014. Climate model benchmarking with glacial and mid-Holocene climates. Clim. Dyn. 43, 671–688. http://dx.doi.org/10.1007/s00382-013-1922-6.
Izumi, K., Lézine, A.M., 2016. Pollen-based biome reconstructions over the past 18,000 years and atmospheric CO2 impacts on vegetation in equatorial mountains of Africa. Quat. Sci. Rev. 152, 93–103. http://dx.doi.org/10.1016/j.quascirev.2016.09.023.

Jolly, D., Haxeltine, A., 1997. Effect of low glacial atmospheric CO2 on tropical African montane vegetation. Science 276, 786–788. http://dx.doi.org/10.1126/science.276.5313.786.
Kageyama, M., et al., 2013. Mid-Holocene and last glacial maximum climate simulations with the IPSL model: part II: model-data comparisons. Clim. Dyn. 40 (9–10), 2469–2495. http://dx.doi.org/10.1007/s00382-012-1499-5.
Kalnay, E., et al., 1996. The NCEP/NCAR 40-year reanalysis project. Bull. Am. Meteorol. Soc. **77**, 437–471. http://dx.doi.org/10.1175/1520-0477. 077 < 0437:TNYRP > 2.0.CO;2 (1996).
Krinner, G., et al., 2005. A dynamic global vegetation model for studies of the coupled atmosphere-biosphere system. Glob. Biogeochem. Cycles 19, GB1015. http://dx.doi.org/10.1029/2003GB002199.
Kutzbach, J.E., 1981. Monsoon climate of the early Holocene: climate experiment with the Earth's orbital parameters for 9000 years ago. Science 214, 59–61. http://dx.doi.org/10.1126/science.214.4516.59.
Lambeck, K., Chappell, J., 2001. Sea level change through the last glacial cycle. Science 292, 679–686. http://dx.doi.org/10.1126/science.1059549.
Lambeck, K., Yokoyama, Y., Purcell, T., 2002. Into and out of the Last Glacial Maximum: sea-level change during Oxygen Isotope Stages 3 and 2. Quat. Sci. Rev. **21** (1), 343–360. http://dx.doi.org/10.1016/S0277-3791(01)00071-3.
Larrasoaña, J., Roberts, A., Rohling, E.J., 2013. Dynamics of Green Sahara periods and their role in Hominin evolution. PLoS ONE **8** (10), e76514. http://dx.doi.org/10.1371/journal.pone.0076514.
Lattanzi, F.A., 2010. C3/C4 grasslands and climate change. In Grassland in a changing world. In: Proceedings of the 23rd General Meeting of the European Grassland Federation, Kiel, Germany, 29th August-2nd September 2010. Mecke Druck und Verlag, pp. 3–13.
Levis, S., Foley, J.A., Pollard, D., 1999. CO2, climate, and vegetation feedbacks at the last glacial maximum. J. Geophys. Res. 104, 31191–31198. http://dx.doi.org/10.1029/1999JD900837.
Ludwig, P., et al., 2016. Regional atmospheric circulation over Europe during the last glacial maximum and its links to precipitation. J. Geophys. Res. Atmos. 121, 2130–2145. http://dx.doi.org/10.1002/2015JD024444.
Ludwig, P., et al., 2017. Impacts of surface boundary conditions on regional climate model simulations of European climate during the last glacial maximum. Geophys. Res. Lett. 44, 5086–5095. http://dx.doi.org/10.1002/2017GL073622.
Maier, A., et al., 2016. Demographic estimates of hunter–gatherers during the Last Glacial Maximum in Europe against the background of palaeoenvironmental data. Quat. Int. **425**, 49–61. http://dx.doi.org/10.1016/j.quaint.2016.04.009.
Marchant, R., et al., 2009. Pollen-based biome reconstructions for Latin America at 0, 6000 and 18 000 radiocarbon years. Clim. Past 5, 725–767. http://dx.doi.org/10.5194/cp-5-725-2009.
Mix, A.C., Bard, E., Schneider, R., 2001. Environmental processes of the ice age: Land, oceans, glaciers (EPILOG). Quat. Sci. Rev. **20**, 627–657. http://dx.doi.org/10.1016/S0277-3791(00)00145-1.
Oster, J.L., et al., 2015. Steering of westerly storms over western north America at the last glacial maximum. Nat. Geosci. 8, 201–205. http://dx.doi.org/10.1038/ngeo2365.
Parton, W.J., et al., 1993. Observations and modeling of biomass and soil organic matter dynamics for the grassland biome worldwide. Glob. Biogeochem. Cycles 7, 785–809. http://dx.doi.org/10.1029/93GB02042.
Peltier, W.R., Argus, D.F., Drummond, R., 2015. Space geodesy constrains ICE age terminal deglaciation: the global ICE-6G_C (VM5a) model. J. Geophys. Res. 120, 450–487. http://dx.doi.org/10.1002/2014JB011176.
Pickett, E.J., et al., 2004. Pollen-based reconstructions of biome distributions for Australia, Southeast Asia and the Pacific (SEAPAC region) at 0, 6000 and 18,000 14C yr BP. J. Biogeogr. 31, 1381–1444. http://dx.doi.org/10.1111/j.1365-2699.2004.01001.x.
Polley, H.W., Johnson, H.B., Marinoj, B.D., Mayeux, H.S., 1993. Increase in C3 plant water-use efficiency and biomass over glacial to present CO2 concentrations. Nature 361, 61–64. http://dx.doi.org/10.1038/361061a0.
Prentice, I.C., Webb III, T., 1998. BIOME 6000: reconstructing global mid-Holocene vegetation patterns from palaeoecological records. J. Biogeogr. **25**, 997–1005. http://dx.doi.org/10.1046/j.1365-2699.1998.00235.x.
Prentice, I.C., et al., 2000. Mid-Holocene and glacial-maximum vegetation geography of the northern continents and Africa. J. Biogeogr. 27, 507–519. http://dx.doi.org/10.1046/j.1365-2699.2000.00425.x.
Raddatz, T.J., et al., 2007. Will the tropical land biosphere dominate the climate – carbon cycle feedback during the twenty-first century? Clim. Dyn. 29, 565–574. http://dx.doi.org/10.1007/s00382-007-0247-8.
Ray, N., Adams, J.M., 2001. A GIS-based Vegetation Map of the World at the Last Glacial Maximum (25,000–15,000 BP). Internet Archaeology 11. http://dx.doi.org/10.11141/ia.11.2.
Shao, Y., et al., 2018. Vegetation Cover for Last Glacial Maximum. Mendeley Data, v1. http://dx.doi.org/10.17632/cr269zdybh.1.
Simonis, D., Hense, A., Litt, T., 2012. Reconstruction of late glacial and early Holocene near surface temperature anomalies in Europe and their statistical interpretation. Quat. Int. 274, 233–250. http://dx.doi.org/10.1016/j.quaint.2012.02.050.
Skoglund, P., et al., 2012. Origins and genetic legacy of Neolithic farmers and hunter-gatherers in Europe. Science 336, 466–469. http://dx.doi.org/10.1126/science.1216304.
Strandberg, G., et al., 2011. High-resolution regional simulation of last glacial maximum climate in Europe. Tellus A: Dynamic Meteorology and Oceanography 63 (1), 107–125. http://dx.doi.org/10.1111/j.1600-0870.2010.00485.x.
Street-Perrott, F.A., Marchand, D.S., Roberts, N., Harrison, S.P., 1989. Global lake-level variations from 18,000 to 0 years ago: A palaeoclimate analysis (No. DOE/ER/60304-H1). Oxford Univ. (UK). Geography School.
Stute, M., et al., 1995. Cooling of tropical Brazil (5°C) during the last glacial maximum. Science 269, 379–383. http://dx.doi.org/10.1126/science.269.5222.379.
Sueyoshi, T., et al., 2013. Set-up of the PMIP3 paleoclimate experiments conducted using an earth system model, MIROC-ESM. Geosci. Model Dev. 6, 819–836. http://dx.doi.org/10.5194/gmd-6-819-2013.
Tans, P., 2018. NOAA/ESRL. online. www.esrl.noaa.gov/gmd/ccgg/trends/ accessed: 8 March 2018.
Tarasov, L., Peltier, R.W., 2002. Greenland glacial history and local geodynamic consequences. Geophys. J. Int. 150, 198–229. http://dx.doi.org/10.1046/j.1365-246X.2002.01702.x.
Tarasov, L., Peltier, R.W., 2003. Greenland glacial history, borehole constraints, and Eemian extent. J. Geophys. Res. **108**, 2143. http://dx.doi.org/10.1029/2001JB001731.
Taylor, K.C., et al., 1997. The Holocene-younger Dryas transition recorded at summit Greenland. Science 278, 825–827. http://dx.doi.org/10.1126/science.278.5339.825.
Tjallingii, R., et al., 2008. Coherent high- and low-latitude control of the northwest African hydrological balance. Nat. Geosci. 1, 670–676. http://dx.doi.org/10.1038/ngeo289.
Tucker, C.J., et al., 2005. An extended AVHRR 8-km NDVI data set compatible with MODIS and SPOT vegetation NDVI data. Int. J. Remote Sens. 26, 4485–4498. http://dx.doi.org/10.1080/01431160500168686.
Voldoire, A., et al., 2013. The CNRM-CM5.1 global climate model: description and basic evaluation. Clim. Dynam. **40** (9–10), 2091–2121. https://link.springer.com/article/10.1007/s00382-011-1259-y.
Wainer, I., et al., 2005. Last Glacial Maximum in South America: Paleoclimate proxies and model results. Geophys. Res. Lett. 32, L08702. http://dx.doi.org/10.1029/2004GL021244.
Wang, X.F., et al., 2017. Hydroclimate changes across the Amazon lowlands over the past 45,000 years. Nature 541, 204–207. http://dx.doi.org/10.1038/nature20787.
Woillez, M., et al., 2011. Impact of $CO_2$ and climate on the Last Glacial Maximum vegetation: results from the ORCHIDEE/IPSL models. Clim. Past 7, 557–577. http://dx.doi.org/10.5194/cp-7-557-2011.
Woodward, F.I., Lomas, M.R., Kelly, C.K., 2004. Global climate and the distribution of plant biomes. Philosophical Transactions of the Royal Society of London B. Biol. Sci. **359**, 1465–1476. http://dx.doi.org/10.1098/rstb.2004.1525.
Wu, H., Guiot, J., Brewer, S., Guo, Z., 2007. Climatic changes in Eurasia and Africa at the last glacial maximum and mid-Holocene: reconstruction from pollen data using inverse vegetation modelling. Clim. Dynam. 29, 211–229. http://dx.doi.org/10.1007/s00382-007-0231-3.
Yukimoto, S., et al., 2012. A new global climate model of Meteorological Research Institute: MRI-CGCM3 – Model description and basic performance. J. Meteorol. Soc. Jpn. **90a**, 23–64. http://dx.doi.org/10.2151/jmsj.2012-A02.